Investigation of the Amplification Properties of Ho:YAG Single Crystal Fiber

Yuan Li[a], Zeyu Zhang[a], Ian Buckley[a], Jerome K. Miller[a], Eric G. Johnson*[a], Craig D. Nie[b], James A. Harrington[b], and Ramesh Shori[c]

[a]The Holcombe Department of Electrical and Computer Engineering, Center for Optical Materials Science and Engineering Technologies (COMSET), Clemson University, Clemson, South Carolina 29634, USA

[b]Department of Material Science and Engineering, Rutgers University, Piscataway, NJ 08854, USA

[c]SPAWAR System Center, Advanced Concepts Group, San Diego, CA 92152 USA

*Corresponding author: ejohns8@clemson.edu

ABSTRACT

0.5% Holmium (Ho) doped YAG single crystal fiber (SCF) was fabricated using the laser heated pedestal growth (LHPG) method and amplification properties of the fabricated Ho:YAG SCF were studied. The relatively large length-to-diameter ratio provides guiding for both the pump and signal beams propagating in the SCF. The propagation and gain of signals with different modes were studied. A numerical method based on finite difference (FD) beam propagation method (BPM) combined with the rate equations was developed for theoretical simulation. The results are encouraging to demonstrate the advantages of SCF for its fiber-like beam guiding property and solid state material gain property. The simulation tool provides details about how the fiber shape and launched mode affect the gain and output beam shape as well as predicts the amplification behavior of such unique specialty fibers.

Keywords: Laser, Holmium, YAG, optical amplifier, single crystal, solid state

1. INTRODUCTION

Merging the excellent mechanical advantages of oxide crystals and the superior thermal management capability of optical fiber geometry, rare-earth doped single crystal fibers (SCF) can potentially produce hundreds of watts of output power. Such potential meets the solid state laser industry's needs towards smaller source crystals and higher power demands. Therefore, a lot of effort has been and will be put into studying SCF with various rare earth dopants and different host materials such as yttrium aluminum garnet (YAG) and sapphire. So far, chromium (Cr), erbium (Er), ytterbium (Yb) and neodymium (Nd) doped SCF with diameters ranging from 120 to 330 μm using yttrium aluminum garnet (YAG) as the host material have been successfully fabricated using the LHPG method [1-5]. Square waveguide Yb:YAG SCF with core diameter as small as 40 μm has been made using precision polishing and crystal bonding processes [6]. To date both CW and pulse amplifiers/lasers with doped-YAG SCF up to 250 W have been demonstrated. Besides the aforementioned dopants, holmium (Ho) and thulium (Tm) are two other important dopants. Ho and Tm doped oxide crystals operate at eye-safe 2 μm spectral region which is applicable to medical applications, atmospheric sensing and coherent radar [7]. The spectroscopy and laser performance of bulk Ho:YAG and Tm:YAG (both single crystal and ceramic) have been widely studied. However, studies investigating SCF utilizing similar materials are relatively new, especially those on their potential in laser power amplification and scaling as a guided gain block.

In previous papers, the spectroscopic properties, including absorption and emission spectrum between 1.9-2.1μm and small-signal gain properties, of Ho:YAG SCF grown using the LHPG method are studied [8, 9]. The large length-to-diameter ratio of the SCF samples assure multiple total internal reflection (TIR) bounces so the light guiding properties can be factored into the performance and be differentiated from well-known bulk material performance. So far, not much effort has been put into studying the beam propagation in the SCF along with signal gain behaviors, either experimentally or theoretically. Experimentally, due to the limitation of fabrication techniques, current SCF is still highly multi-mode waveguide. Most of the current works on SCF amplifiers are still treating the SCF as a bulk. Theoretically, the large simulation area (large SCF cross section diameter) and complicated mode behavior during propagation increase the simulation difficulties.

Solid State Lasers XXIV: Technology and Devices, edited by W. Andrew Clarkson, Ramesh K. Shori,
Proc. of SPIE Vol. 9342, 934205 · © 2015 SPIE · CCC code: 0277-786X/15/$18 · doi: 10.1117/12.2086858

In this work, we compare the amplification properties of two Ho:YAG SCF samples. To understand the results better, a numerical tool based on finite difference (FD) beam propagation method (BPM) combined with transversally resolved (TR) rate equations was developed for theoretical simulation. The simulation tool provides details on how different modes propagate in the SCF, how their gain properties vary and how SCF geometry impacts the mode quality.

2. EXPERIMENT: SETUP AND RESULT

Two 0.5% Ho:YAG SCF samples are studied in the experiment. Both are fabricated using the LHPG method from the same source crystal. One sample has an average diameter of approximately 240 μm and a length of 11.8 cm. Another sample has an average diameter of approximately 400 μm and a length of 10.1 cm. Both samples are end polished.

The experimental setup is shown in Fig. 1. A co-pumping scheme is chosen to be consistent with simulation modeling. The pump laser is a Tm:fiber laser (modified from a Nufern Tm:fiber amplifier) at 1932 nm with a maximum output power of 7 W and a spectral linewidth of 3 nm. The seed laser is delivered by a 9/125 single mode fiber (SMF) to ensure the best mode quality by coupling the output power from a tunable IPG laser into the SMF. L1-L4 are AR-coated lens for the 2 μm region, F1 and F2 are dielectric mirrors which are highly reflective at the signal wavelength and highly transmissive at 1932 nm. The focal length of L2 and L3 are chosen so that the focused seed laser beam size at the facet of the SCF has a radius of approximately 77 μm, which approximately matches the fundamental mode size of the SCF sample with a diameter of 240 μm. A power meter and an IR camera are used to measure the amplifier seed power and to image the output signal beam, respectively.

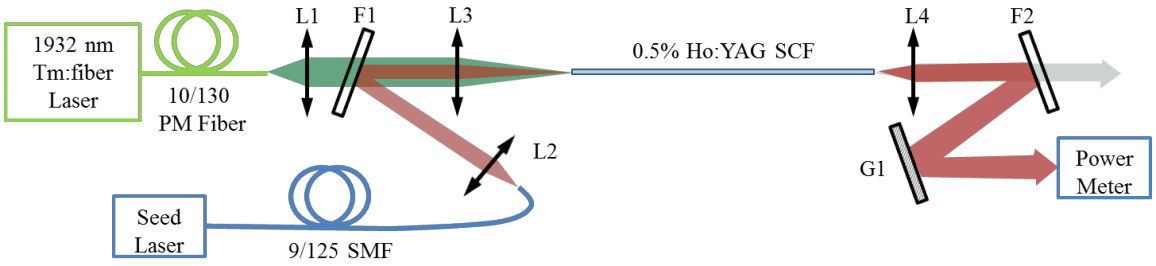

Figure 1. Experimental setup for measuring the small signal gain of the Ho:YAG SCF using a co-pumping scheme. Optical Components: L1-L4 (AR-coated lenses), F1 and F2 (dielectric filters), G1 (gold mirror for reflecting the amplified signal).

Based on the intensity of the emission spectrum, a 2090 nm signal was chosen for measurement of the small signal gain. Signals of incident powers of 87 mW, 143 mW and 226 mW were chosen to evaluate the gain as a function of pump power; the results for both samples are plotted in Fig. 2. As we can see, for the same pump power, signal with smaller incident power experiences higher gain, which agrees with small signal gain and gain saturation effect. This is true for both samples. Additionally, the comparison between results of the two samples shows that the SCF sample with smaller diameter yields higher gain for same pump power and same seed power. Since the length of the two samples is similar, the pump power intensity as well as the effective gain coefficient, will be inversely proportional to the SCF cross-section area [10]. Based on the diameter difference between our samples, ideally the SCF with a 240 μm diameter is expected to show a gain of 2.8 times higher than the SCF with a 400 μm diameter under the same pumping condition. However, due to experimental constraints as well as slightly different fiber parameters, the difference in gain is not as high as expected.

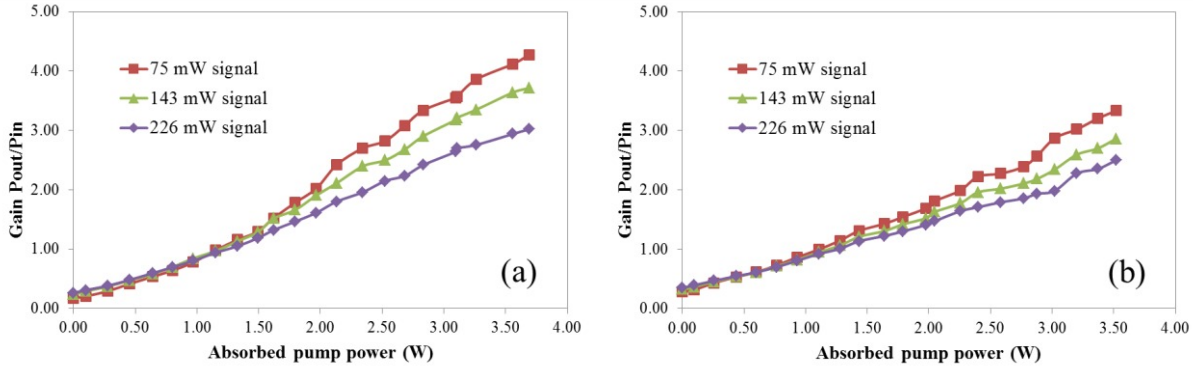

Figure 2. The measured gain for a 2090 nm signal with different input powers vs. absorbed pump power: (a) sample with a diameter of approximately 240 μm and a length of 11.8 cm; (b) sample with a diameter of approximately 400 μm and a length of 10.1 cm.

3. NUMERICAL MODEL

Since SCF is a highly multimode waveguide, how the beam propagates in the SCF will depend on the incident beam shape, launching condition as well as SCF geometry. Thus, a 3-D beam propagation model will be needed to predict the output mode. The pump and signal beams will have different intensity distribution at the same cross section all along the SCF, which means the pump and signal beam overlap will be different along the SCF. Models based on consistent pump and signal beam overlap, either for fiber amplifier or bulk amplifier, are not suitable for this scenarios. Consequently, transversally resolved (TR) rate equations will be combined with FD-BPM to solve the signal gain. In the following discussion, a brief explanation on the FD-BPM method and the TR rate equation set will be present along with the simulation procedure. This model follows close to the model used in [11] with necessary modifications.

Assume the coupling between the two polarizations is weak and negligible, which is true for most optical waveguide. Furthermore, assuming a weakly guiding condition, the vector wave equation can be reduced down to scalar wave equation [12, 13]:

$$(\frac{\partial^2}{\partial x^2}+\frac{\partial^2}{\partial y^2}+\frac{\partial^2}{\partial z^2})E+k^2n^2(x,y,z)E=0 \tag{1}$$

If one-way propagation (in $+z$ direction) is assumed and the electric field $E(x, y, z)$ can be separated into two parts: the axially slowly varying envelope term $\phi(x, y, z)$ and the fast varying phase term $exp(-jkn_0z)$, then the electric filed can be expressed as:

$$E(x,y,z)=\phi(x,y,z)e^{-jkn_oz} \tag{2}$$

Where n_0 is a reference refractive index close to the effective index of the beam in the SCF, and n_0 is chosen so that the envelope varies slowly in the propagation direction. Substituting Eq. (2) into (1), a one-way wave equation is obtained:

$$\frac{\delta\phi}{\delta z}=-j\frac{1}{2kn_o}\nabla^2\phi-j\frac{k}{2n_o}\left[n^2(x,y,z)-n_o^2\right]\phi \tag{3}$$

Where,

$$\nabla^2=\frac{\partial^2}{\partial x^2}+\frac{\partial^2}{\partial y^2} \tag{4}$$

Eq. (3) can be solved numerically by FD approximation at a small distance Δz, by iterating the process the beam propagates in the$+z$ direction until the desired length is reached.

Then the TR steady-state rate equations are briefly presented, which follows close to the form in [14, 15]. The equations are assuming a most general two-level energy band structure, which works for either a four-level or a three-level

transition which may or may not include excited state absorption (ESA). It is also assumed that nonradiative decays are very fast and the transition time can be ignored compared to laser upper level lifetime τ. In order to be compatible with BPM, the TR rate equations are discretized,

$$\frac{N_{2(m,k)}(z)}{N_{1(m,k)}(z)} = \frac{\dfrac{[P_p^+(z)+P_p^-(z)]\sigma_{ap}\Gamma_{p(m,k)}}{h\nu_p A_{(m,k)}} + \dfrac{P_s^+(z)\sigma_{as}\Gamma_{s(m,k)}}{h\nu_s A_{(m,k)}}}{\dfrac{[P_p^+(z)+P_p^-(z)]\sigma_{ep}\Gamma_{p(m,k)}}{h\nu_p A_{(m,k)}} + \dfrac{1}{\tau} + \dfrac{P_s^-(z)]\sigma_{es}\Gamma_{s(m,k)}}{h\nu_s A_{(m,k)}}} \tag{5}$$

$$\frac{dP_s^+(z)}{dz} = \sum_m \sum_k \left[\sigma_{es} N_{2(m,k)}(z) - \sigma_{as} N_{1(m,k)}(z)\right]\Gamma_{s(m,k)} P_s^+(z) - \alpha_s P_s^+(z) \tag{6}$$

$$\pm\frac{dP_p^\pm(z)}{dz} = \sum_m \sum_k \left[\sigma_{ep} N_{2(m,k)}(z) - \sigma_{ap} N_{1(m,k)}(z)\right]\Gamma_{p(m,k)} P_p^\pm(z) - \alpha_p P_p^\pm(z) \tag{7}$$

$$A_{(m,k)} = \Delta x \cdot \Delta y \tag{8}$$

$$\Gamma = \frac{\psi(m\Delta x, k\Delta y)}{\sum_m \sum_k \psi(m\Delta x, k\Delta y)} \tag{9}$$

Where $N_{(m,\,k)}$ is the ion concentration at a transversal point (m, k), 1 and 2 stands for lasing lower and upper levels, respectively. P_s is signal power and P_p is pump power. The + sign and – sign represent the beam propagation direction, either $+z$ or $-z$. In our case both pump and signal propagate in the $+z$ direction. σ_{ap} and σ_{ep} are the absorption and emission cross sections at the pump wavelength, respectively. Similarly, σ_{as} and σ_{es} are the absorption and emission cross sections at the signal wavelength, respectively. Additionally, h is the Planck constant, ν_p is the pump frequency, ν_s is the signal frequency, α_p and α_s are the loss/attenuation coefficients of the pump and signal through the SCF, respectively. $\Gamma_{(m,\,k)}$ is the power filling factor at a transversal point (m, k) and the discretized area of a point is A(m, k).

As a summary, the model operates based on the following steps:

Step 1, define input signal and pump beam E field distributions and powers.

Step 2, propagate both beams using FD-BPM separately over Δz distance.

Step 3, calculate $\Gamma_{s(m,\,k)}$ and $\Gamma_{p(m,\,k)}$ for each point and solve eq. (5-7) for powers.

Repeat step 2 and step 3 until the end of the SCF is reached.

4. SIMULATION RESULTS AND DISCUSSION

Fig. 3 shows the closest simulation result to the experiment data for a 75 mW 2090 nm signal being amplified in the Ho:YAG SCF with 240 μm in diameter. The parameters for the simulation are as follows: N=0.42×10^{26} m^{-3} (The actual doping concentration is smaller than 0.5% due to segregation effect. This number is chosen so that it best fits the experimental results.), σ_{ap}=0.51×10^{-20} cm^2, σ_{ep}=0.41×10^{-20} cm^2, σ_{as}=0.23×10^{-20} cm^2, σ_{es}=1.2×10^{-20} cm^2, τ=8.5 ms [14], α_p =0.07 cm^{-1}, and α_s =0.03 cm^{-1}. The fitted pump loss α_p is higher than the measured scattering loss of the SCF (approximately 0.02 cm^{-1}), which indicates the pumping efficiency is probably not optimized.

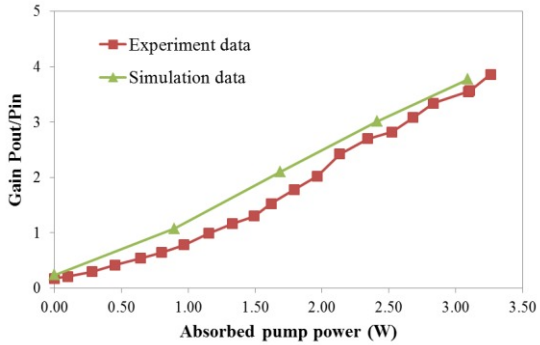

Figure 3. The simulation results compared to the experimental results for the Ho:YAG SCF sample . The experimental data is for the 75 mW input signal amplified in SCF with a 240 μm diameter.

A Gaussian beam with $1/e^2$ width of 77 μm is used as the input beam for propagation, the simulated input and output beam intensity distribution are shown in Fig. 4(a) and 4(b). Due to the slight mismatch between the input mode and the fundamental mode of the SCF (which is 88 μm in radius by numerical simulation), Multi-mode interference (MMI) effect is observed due to the mode coupling to different radial modes that are supported in the SCF since it is a highly multi-mode waveguide.

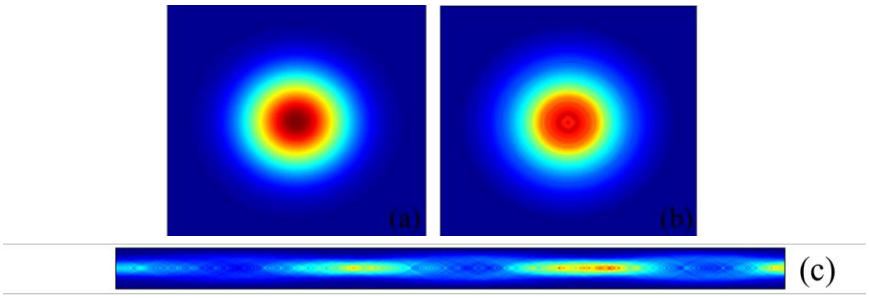

Figure 4. (a) The ideal 77 μm Gaussian input intensity distribution. (b) Simulated output beam intensity distribution after the input beam propagating along the SCF. The diameter of the SCF used in the simulation is 240 μm, the length is 11.8 cm. An ideal cylindrical mode is assumed. (c) A slice of the intensity plot along the propagating axis.

The cross section along the propagating axis of the SCF is shown in Fig. 4(c). However, the simulation assumes a perfect SCF geometry, with uniform diameter and circular cross section throughout the fiber. The actual SCF cross section shows some asymmetry in geometry, which yields mode mixing and mode quality degradation along the beam propagation. Fig. 5(a) shows the actual SCF geometry. Fig. 5(b) and 5(c) show the simulated output beam intensity of input Gaussian beams with $1/e^2$ width of 77 μm and 10 μm, respectively. As we can see, the 77 μm beam does not degrade too much. However, the 10 μm beam completely loses radial symmetry after propagation. This is because the smaller beam diverges faster and bounces more on the wall; therefore the geometry asymmetry has more impact on a small beam during propagation. However, in our experiment, even with a 77 μm input beam, the output looks similar to Fig. 5(c), which indicates strong mode mixing. For SCF to work as a waveguide, the requirements on the SCF geometry symmetry and diameter uniformity need to be reasonably strict, as those on the mode launching condition.

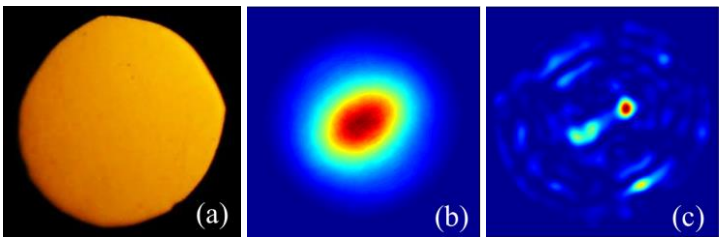

Figure 5. (a) The microscope image of the SCF cross section (polished end facet). (b) The simulated output beam intensity distribution of a 77 μm Gaussian input beam using the actual fiber shape. (c) The simulated output beam intensity distribution of a 10 μm Gaussian input beam using the actual fiber shape.

5. CONCULSION

The performance of Ho:YAG SCF as a gain waveguide is studied and a 3-D BPM model with gain block incorporated is used for simulation. Due to the geometry imperfections of the SCF, maintaining the mode quality while propagating along the SCF is difficult. However, the simulation shows the feasibility of guiding the input beam and predicting the output beam. With proper launching conditions, matching the mode size of the SCF and maturing the fabrication method, it is possible to maintain the input beam shape with minimum degradation at the output end of the SCF. This applies not only for the fundamental mode, but also for higher order modes such as a vertex beam. While taking advantage of enhanced thermal management, the relatively long length of the SCF compared to bulk crystal typically used in solid state amplifier (typically a few millimeters) demonstrates the potential of significant power scaling.

ACKNOWLEDGEMENTS

Funding for this research was provided by the HEL-JTO and through ARO W911NF-12-1-0536 and FA9550-10-1-0543.

REFERENCES

[1] X. Délen, S. Piehler, J. Didierjean, N. Aubry, A. Voss, M. Ahmed, T. Graf, F. Balembois, and P. Georges, "250 W single-crystal fiber Yb:YAG laser," Opt. Lett. 37, 2898-2900 (2012).
[2] N. Ter-Gabrielyan, V. Fromzel, X. Mu, H. Meissner, and M. Dubinskii, "High efficiency, resonantly diode pumped, double-clad, Er:YAG-core, waveguide laser," Opt. Express 20, 25554-25561 (2012).
[3] X. Délen, I. Martial, J. Didierjean, N. Aubry, D. Sangla, F. Balembois, P. Georges, "34 W continuous wave Nd:YAG single crystal fiber laser emitting at 946 nm," Applied Physics B. 104, 1-4 (2011).
[4] P. Shi, I. Watson, and J. Sharp, "High-concentration Er:YAG single-crystal fibers grown by laser-heated pedestal growth technique," Opt. Lett. 36, 2182-2184 (2011).
[5] Ishibashi, Shigeo, and Kazunori Naganuma. "Mode-locked operation of Cr 4+: YAG single-crystal fiber laser with external cavity." Optics express 22.6 (2014): 6764-6771.
[6] Mu, X., Meissner, S., Meissner, H., & Yu, A. W. (2014). High efficiency Yb: YAG crystalline fiber-waveguide lasers. Optics letters, 39(21), 6331-6334.
[7] B. Walsh, "Review of Tm and Ho Materials; Spectroscopy and Lasers," Laser Physics, 19, 4, 855–866 (2009).
[8] Li, Yuan, Eric G. Johnson, Craig D. Nie, James A. Harrington, and Ramesh Shori. "Ho: YAG single crystal fiber: fabrication and optical characterization." Optics express 22, no. 12 (2014): 14896-14903.
[9] Harrington, J. A., Nie, C. D., Cloos, E. F., Rand, S. C., Li, Y., & Johnson, E. (2013, October). Single-Crystal, Rare-Earth Doped-YAG Fibers Grown by the Laser Heated Pedestal Growth Technique. In Frontiers in Optics (pp. FTu4B-4). Optical Society of America.
[10] Brignon, A., Feugnet, G., Huignard, J. P., & Pocholle, J. P. (1998). Compact Nd: YAG and Nd: YVO 4 amplifiers end-pumped by a high-brightness stacked array. Quantum Electronics, IEEE Journal of, 34(3), 577-585.
[11] Jauregui, Cesar, Tino Eidam, Jens Limpert, and Andreas Tünnermann. "Impact of modal interference on the beam quality of high-power fiber amplifiers." Optics express 19, no. 4 (2011): 3258-3271.
[12] Okamoto, Katsunari. Fundamentals of optical waveguides. Academic press, 2010.
[13] Xu, C. L., and W. P. Huang. "Finite-difference beam propagation method for guide-wave optics." Progress In Electromagnetics Research, PIER 11 (1995): 1-49.
[14] M. Schellhorn and A. Hirth, "Modeling of Intracavity-Pumped Quasi-Three-Level Lasers," Quantum Electronics, IEEE Journal of , 38. 11. 1455-1464, (2002).
[15] Hardy, Amos, and R. Oron. "Signal amplification in strongly pumped fiber amplifiers." Quantum Electronics, IEEE Journal of 33.3 (1997): 307-313.